
More Reliable AI Solution: Breast Ultrasound Diagnosis Using Multi-AI Combination

Jian Dai¹, Shuge Lei^{1,2}, Licong Dong³, Xiaona Lin³, Huabin Zhang⁴, Desheng Sun^{3*}, Kehong Yuan^{1*}

¹ Graduate School at Shenzhen, Tsinghua University, Shenzhen, China

² Computer Science and Engineering, University of South Carolina, SC, United States

³ Ultrasound department, Shenzhen Hospital of Peking University, Shenzhen, China

⁴ Ultrasound department, Beijing Tsinghua Changgeng Hospital, Beijing, China

Corresponding author: Kehong Yuan (yuankh@sz.tsinghua.edu.cn), Desheng Sun (szdssun1@126.com).

ABSTRACT *Objective:* Breast cancer screening is of great significance in contemporary women's health prevention. The existing machines embedded in the AI system do not reach the accuracy that clinicians hope. How to make intelligent systems more reliable is a common problem. *Methods:* 1) Ultrasound image super-resolution: the SRGAN super-resolution network reduces the unclarity of ultrasound images caused by the device itself and improves the accuracy and generalization of the detection model. 2) In response to the needs of medical images, we have improved the YOLOv4 and the CenterNet models. 3) Multi-AI model: based on the respective advantages of different AI models, we employ two AI models to determine clinical results cross validation. And we accept the same results and refuses others. *Results:* 1) With the help of the super-resolution model, the YOLOv4 model and the CenterNet model both increased the mAP score by 9.6% and 13.8%. 2) Two methods for transforming the target model into a classification model are proposed. And the unified output is in a specified format to facilitate the call of the multi-AI model. 3) In the classification evaluation experiment, concatenated by the YOLOv4 model (sensitivity 57.73%, specificity 90.08%) and the CenterNet model (sensitivity 62.64%, specificity 92.54%), the multi-AI model will refuse to make judgments on 23.55% of the input data. Correspondingly, the performance has been greatly improved to 95.91% for the sensitivity and 96.02% for the specificity. *Conclusion:* Our work makes the AI model more reliable in medical image diagnosis, and it performs well in the detection of breast lesions. *Significance:* 1) The proposed method makes the target detection model more suitable for diagnosing breast ultrasound images. 2) It provides a new idea for artificial intelligence in medical diagnosis, which can more conveniently introduce target detection models from other fields to serve medical lesion screening.

Keywords artificial intelligence algorithm, breast lesions, breast ultrasound, super-resolution, target detection, multi-AI model, cloud-based

I. INTRODUCTION

Breast cancer has become the biggest threat to female health, and it is the malignant tumor that caused the highest incidence and the second-highest mortality rate among women¹. For females worldwide, the cumulative risks to age 75 are 5.03%². Early screening and diagnosis are key factors in reducing the mortality rate of breast cancer³. Formerly used in clinical practice for decades, breast ultrasonography has gained continuous technological breakthroughs and eventually replaced mammography in detecting breast cancer⁴. However, ultrasonography relies heavily on the doctor's experience, operating methods, and equipment parameters. The skills of the doctors will greatly influence the diagnosis results⁵. Also, the resolution of ultrasound inspection equipment varied greatly in China. Diagnostic accuracy is affected by doctors' skills (the increasing workload of sonographers, the fatigue caused by long-term reading, the inexperience of young physicians, etc.)

and ultrasound image quality. Diagnostic errors go against the prevention and treatment of breast cancer and could seriously ruin patients' physical and mental health. With the development of artificial intelligence, AI-based computer-aided diagnostic systems show great promise in breast diagnosis.

Currently, many organizations are developing computer-aided diagnostic systems based on artificial intelligence technology for breast diagnosis. Although the current research has made significant progress, such systems face many challenges. The complexity of algorithms is constantly increasing due to the high accuracy requirements for medical diagnosis. This requires ultra-high computing capability. Most current systems use AI-embedded devices, which have low computing capability for real-time calculations⁶, thus cannot empower the complex algorithms. To solve this problem, computing in the cloud gained increasing popularity⁷.

Moreover, the current diagnostic systems always have problems in dealing with ultrasound devices with different resolutions. One system usually expertized at a certain range of resolutions of medical images, which limited the systems' generalization and scalable ability. Besides, most current systems are based on a single traditional detection model. To the best of our knowledge, multi-AI models are seldomly employed in such detection tasks.

To address the above challenges in ultrasound breast examination, we develop a more reliable ultrasonic computer-aided diagnosis system --- Multi-AI Combination detection system. We employed the SRGAN super-resolution network to reduce the problem of unclear ultrasound images caused by the device itself and improve the detection model's accuracy and generalization. A Multi-AI model with high computing power machines in the cloud is employed to help doctors reduce workload with a low misdiagnosis rate.

II. RELATED WORK

Super-resolution techniques. The goal of Super-Resolution (SR) methods is to recover a High Resolution (HR) image from one or more Low Resolution (LR) input images. Two kinds of super-resolution methods for medical images are widely used, e.g., interpolation-based super-resolution reconstruction algorithm⁸, and learning-based super-resolution reconstruction algorithm⁹. The application of neural networks has greatly improved the algorithm's speed to find the optimal solution, and various experimental results have achieved good results in evaluation indicators and visual perception.

SRGAN is the first model to reconstruct super-resolution images using convolutional neural network. It employed three-layer convolutional neural networks to learn the mapping relationship between high-resolution images and low-resolution images to guide the reconstruction¹⁰. SRGAN presented a super-resolution generative adversarial network, which is the first framework to recover photo-realistic natural images from $4 \times$ down sampling¹¹. In the experiment, we use the super-resolution model as part of the image preprocessing to improve the clarity of the image from the ultrasound device, thereby achieving to improve the accuracy of the target detection

Model Compression. A modern detector is usually composed of two parts, a backbone which is pre-trained on ImageNet and a head which is used to predict classes and bounding boxes of objects¹². According to the difference of the head, it can be divided into two categories: One-stage object detector and a two-stage object detector. For two-stage detectors, they combine the steps of classifying the box proposals through a CNN (convolutional neural network) model and refining the coordinates with the sliding window manner¹³, such as RCNN¹⁴, fast R-CNN¹³, faster R-CNN¹⁵, etc. For one-stage object detectors, the most representative models are YOLO^{11,12,16,17}, SSD¹⁸, RetinaNet¹⁹. They predict confidences and locations for multiple objects based on the whole feature map directly^{20,24}. Furthermore, anchor-free one-stage detectors are developed during the recent years. CenterNet²¹ and CornerNet²² detect targets by matching key points instead of the anchor frame principle, which improved accuracy and speed. In our work, we have made some improvements between the head and backbone to meet the classification function for ultrasound images.

Medical image and multi-AI model. The application of deep learning to medical images has caught great attentions. The common steps of such deep learning systems are as follows: organize the lesion data set, select the target detection model, adjust the parameters of the model, and transplant it to embedded devices or mobile workstations^{20,24}. The algorithm engineers usually pay their efforts to

optimize the model, yet less attention to help medical workers reduce their workload. On the one hand, the existing models work independently; the latter model replaces the old model. Combining these models can be a new perspective. On the other hand, different from general target detection, medical workers do not care too much about indicators such as mAP. They only care about whether this tool will misdiagnose patients. To some extent, the model can help doctors complete the initial screening work.

The Multi-AI model is different from traditional parameter tuning or modular splicing. It provides a new perspective to quickly introduce natural image detection models. We do not replace the existing high-precision detection models but combine them together. Different models analyze the same picture together, just like an expert consultation, which fully considers the individual evaluation of each model.

III. METHOD

A. THE MULTI-AI MODEL

The common improvements of deep learning models are to make some improvements between the head and backbone¹². To some extent, these optimizations will improve the accuracy of the model. As shown in Fig.1, our experiment combines the YOLOv4 model and the CenterNet model to evaluate the pathological images. The principles are similar when combining more models for analysis.

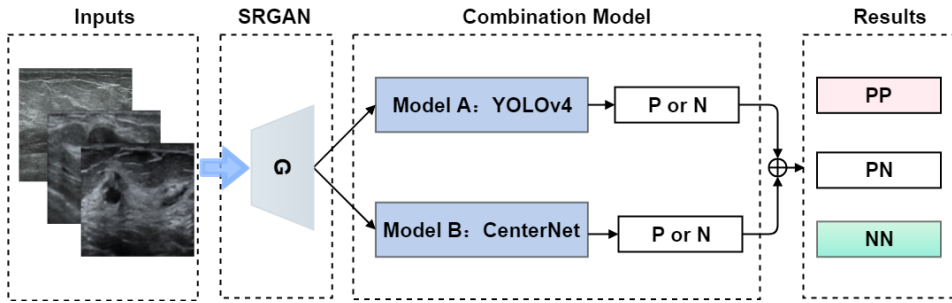


Fig. 1. The framework of the multi-AI model

As shown in Figure 1, the Multi-AI model does not mark all pictures. Only when the two sub-models agree on their opinions will they give a definite evaluation; the others will be left to the doctors for further judgement. Therefore, the output is actually the affirmative result of multiple models, which reduces the risk as much as possible. We define PP as diseased, NN as disease-free, and PN means unable to judge.

Here we averagely weight the output of the two sub-models as shown in Eqn. (1):

$$P_{multi-AI} = P_{yolov4} + P_{centerernet} \quad (1)$$

After adjusting the appropriate threshold (C_1 and C_2) according to Eqn. (2), the model can achieve the function of Figure 5.

$$\begin{cases} \text{if } P_{multi-AI} \gg C_1, \text{Result} = PP \\ \text{if } P_{multi-AI} \ll C_2, \text{Result} = NN \\ \text{others}, \text{Result} = PN \end{cases} \quad (2)$$

Of course, we can also try the following operations in a joint system composed of multiple models:

$$P_{multi-AI} = \sum_{i=1}^n \lambda_i P_i \quad (3)$$

In Eqn. (3), λ_i is the reliability coefficient of the sub-model. Adjusting the weights of different sub-models can make the model more flexible and stable. Combined with Eqn. (2), it is also very convenient to adjust n to $n+1$ in multi-AI model.

We have analyzed how to use a target detection network to complete the classification task, and we will implement similar functions in this section. Our model pays more attention to the existence rather than the location of the lesions. Paying more attention to the accuracy reduced the importance of marking the anchor position.

B. TARGET DETECTION MODEL

The structure of target detection model and image classification model has many commonalities. When analysing medical images, these two tasks are performed simultaneously. We should first determine whether the patient has lesion and then locate the lesion.

Obviously, there are two areas worthy of optimization: backbone and head. On the one hand, we can connect the output feature map of the backbone part of the YOLOv4 model to the fully connected layer to output category information (as shown in Figure 4). On the other hand, the output of the detection model itself represents information such as the location of the target (lesion), and we can also use the head output information of the CenterNet model for classification (as shown in Figure 5).

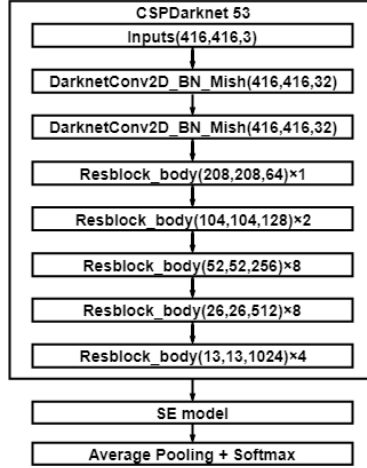


Fig. 2. The combination of the backbone of YOLOv4 and the SENet

In this paper, we embed the SE module at the output of the Dark net. As shown in Figure 2, the channel of the SE module weights the feature map and inputs it to the fully connected layer to realize the function of the classification network. When the classification network determines that the input picture has a lesion, the remaining network of YOLOv4 determine the location of the target frame.

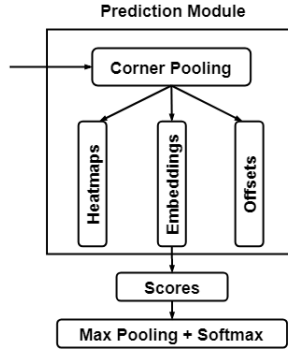


Fig. 3. The head of CenterNet with classification function

As shown in Figure 3, the CenterNet module will output Heatmaps, Embeddings, Offsets after passing the unique angular pooling²¹. Among them, Embeddings contains anchor position and score information in the output of the detection module. We extract the scores in Embedding, which is to

score all possible target boxes of each heatmap in the result. Then we use maximum pooling to obtain the maximum probability of disease in different areas of the heatmap, followed by the Softmax to get two categories. Of course, both improvements of YOLOv4 and CenterNet can be applied to each other. The work we have done is to prepare for the next classification experiment.

C. SUPER-RESOLUTION USED IN OUR EXPERIMENTS

The GAN network consists of a generator model (G) and a discriminative model (D). The G model is responsible for generating data that is as close to the real sample as possible, and the D model is used to score the output result, which is to judge whether the generated sample is true or false. As shown in Fig.4, the input of the G model of the SRGAN network is a low-resolution image I^{LR} , and the high-resolution output image I^{SR} will be used as the input of the D model together with the original image I^{HR} .

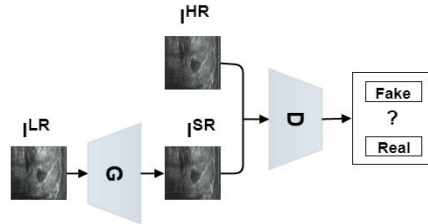


Fig. 4. The framework of SRGAN

When training SRGAN, it uses a four times downsampling factor to obtain low-resolution images and optimizes in an alternating manner to solve the minimum-maximum adversarial problem:

$$\min_{\theta_G} \max_{\theta_D} \mathbb{E}_{I^{HR} \sim p_{\text{train}}(I^{HR})} [\log D_{\theta_D}(I^{HR})] + \mathbb{E}_{I^{LR} \sim p_C(I^{LR})} [\log (1 - D_{\theta_D}(G_{\theta_G}(I^{LR})))] \quad (4)$$

Different from previous works, they defined a novel perceptual loss using high-level feature maps of the VGG network²³, combined with a discriminator that encourages solutions perceptually hard to distinguish from the HR reference images¹⁰. The VGG loss is defined as the Euclidean distance between the feature representation of the reconstructed image $G_{\theta_G}(I^{LR})$ and the reference image I^{HR} :

$$l_{VGG}^{SR} = \frac{1}{W_{i,j}H_{i,j}} \sum_{x=1}^{W_{i,j}} \sum_{y=1}^{H_{i,j}} -(\phi_{i,j}(I^{HR})_{x,y} - \phi_{i,j}(G_{\theta_G}(I^{LR}))_{x,y})^2 \quad (5)$$

The method of independent alternating iterative training makes the two networks oppose to each other. In the end, the goal of the G network can "deceive" the D network, and the G network is what we need.

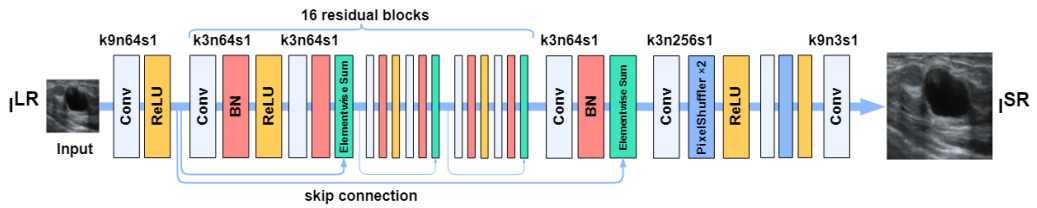


Fig. 5. The architecture of Generator Network with corresponding kernel size (k), number of feature maps (n), and stride (s) indicated for each convolutional layer

The generative network in the experiment was shown in Fig.5. After the input image passed the convolution block, it went through 16 Residual Blocks (RB) with skip connections. Each RB module consists of two convolutional layers with 3×3 filters and a feature map of 64 channels, followed by a batch-normalization layer and ReLU activation.

The output went through the Elementwise-sum module, and the output of RB was connected to the features of the first convolutional layer. The image can be obtained through 2 upsampling blocks

(PixelShuffler) and the last convolutional layer. The scale factor depends on the number (4 used in this article) of upsampling blocks.

D. DATA AND PREPROCESSING

Obtaining medical data has always been a difficult task, and there are no suitable public data set resources. The data set in this paper comes from the database of the Ultrasound Imaging Department of Peking University Shenzhen Hospital. We collected 6,860 pictures, including 2,065 images with benign lesions and 3,495 images with malignant lesions, and 1,300 images without lesions.

Table 1 The dataset used in our experiment

Dataset	Images with benign nodules	Images with malignant nodules	Images without nodules
Training Dataset	1870	3160	0
Validation Dataset	195	335	1300

During data marking, five doctors used the open-source software LabelImg to label these data, which were collected from 2804 patients. In order to ensure the accuracy of the data, one doctor marks the image while the other doctor checks it.

The target detection model must have a target during the training process; only the image with lesion is helpful to the training model. Therefore, as shown in Table 1, we finally selected 5030 lesion images as the training set, and 530 lesion images and 1300 disease-free images as the validation set.

E. METRICS

The purpose of the experiment is to improve the clarity of ultrasound images and improve the detection accuracy of the target detection model. Therefore, the evaluation indicators we use in our experiments are mainly from the field of target detection and digital imagery.

Table 2 The metrics used in the experiments

Evaluation index	Method of calculation
Precision	$\frac{TP}{TP + FP}$
Recall	$\frac{TP}{TP + FN}$
Specificity	$\frac{TN}{TN + FP}$
mAP	Area covered under PR curve
MSE	$MSE = \frac{1}{H \times W} \sum_{i=1}^H \sum_{j=1}^W (X(i, j) - Y(i, j))^2$
PSNR	$PSNR = 10 \cdot \log_{10} \left(\frac{MAX_I^2}{MSE} \right)$
SSIM	$SSIM(x, y) = \frac{(2\mu_x\mu_y + c_1)(2\sigma_{xy} + c_2)}{(\mu_x^2 + \mu_y^2 + c_1)(\sigma_x^2 + \sigma_y^2 + c_2)}$
RTP	The task reduced by AI machine

As shown in Table 2, in order to evaluate the effect of lesion feature detection, we used four indexes: precision, recall, sensitivity, and mAP. As shown in the calculation formula, TP and FN represent the number of positive samples inferred as positive and negative samples, and FP and TN represent the number of negative samples inferred as positive and negative. Precision reflects the model's ability to accurately identify lesion images, and Specificity reflects the model's ability to accurately identify disease-free images. Draw a curve composed of recall score and precision score

on the coordinate axis. The area of the curve represents the AP value, which is usually used to comprehensively measure the accuracy of the detector model. The classification task is not the same as the target detection task. It only makes a judgment on whether it is diseased or not, rather than predicts the location of the lesion in the ultrasound image. Therefore, our experiment is divided into two tasks: image classification and lesion detection; yet, the metrics are the same.

We also defined an RTP indicator (Reduced Task Proportion), which means the workload that the AI-assisted diagnostic device helps doctors reduce. The Multi-AI Model does not make evaluation for every input picture. Only when the evaluations of all sub-models are consistent, the system will give its judgment, and the other pictures will be given to the doctor. Since it only selects certain pictures to make judgments, we use RTP indicators to comprehensively evaluate the practical significance of the model.

IV. RESULTS

A. SUPER RESOLUTION

We need to verify that super-resolution can improve the quality of ultrasound images and improve the effect of lesion detection. Two types of experiments were considered to ensure the reliability of the experiment results: the indicators of the image itself based and the detection effect based.

First, we selected 530 lesion images and 1300 disease-free images as the evaluation data set, and qualitatively evaluated them through PSNR and SSIM indicators, and then introduced MOS indicators as subjective evaluation indicators.

Mean Opinion Score (MOS): The observer makes a subjective evaluation of the image's quality. The larger the value (between 0 and 5), the better the image quality. We compared the evaluation value of the algorithm with the subjective score value from human's judge.

Table 3 Evaluation score of image super-resolution

Size	720×1024	256×256	64×64
PSNR	23.53	24.48	26.97
SSIM	0.5523	0.5592	0.8703
MOS	3.67	3.98	4.12

When evaluating images through qualitative indicators such as PSNR and SSIM, it is necessary to ensure that the contrast images are consistent in size. The output here will be the input of the next target detection model. We analyzed the score of the image in three sizes. As shown in Table 3, when the size of the output image is reduced, the score of the super-resolution image will become higher and closer to the original image. Thus, we use the output with a size of 256×256 as the input of the next target detection model.

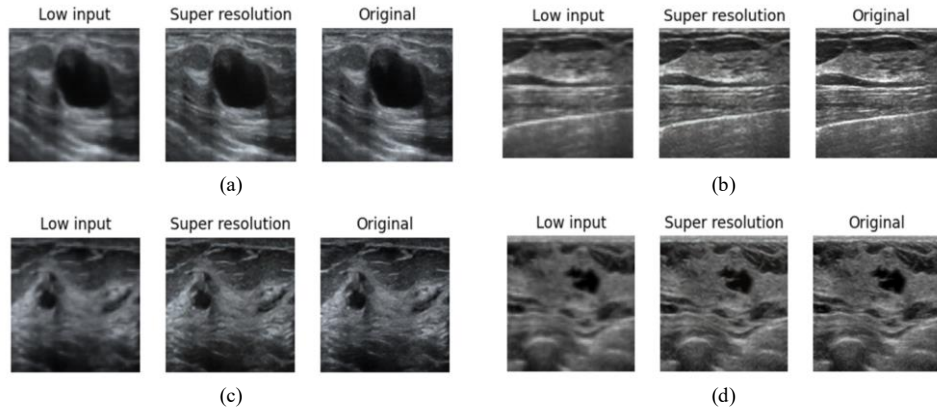


Figure 6 Super-resolution breast ultrasound images

It can be seen from the image that both the lesion (a) or the normal tissue (b), the super-resolution

images have a better recovery effect, and there is no increased noise in some suspected lesion tissue (c) (d).

B. TARGET RECOGNITION

It is very important to verify the inference results after super-resolution processing through an improved target detection model. The current target detection model will not be retrained or directly changed model parameters after being embedded in the device. Therefore, our model training uses the original image of the training set instead of dividing the training set into HR, LR, and SR separately. This also ensures the single variable principle of our experiment and make it more convincing.

In order to avoid the contingency of a single model, we use both YOLOv4 and CenterNet to verify the actual model effect. As an anchor-based model, YOLOv4 added an artificial prior distribution; thus, the predicted value range during training is actually relatively small, which makes anchor-based networks easier to train and more stable. As a keypoint-based method, CenterNet has a larger and more flexible solution space. Getting rid of the amount of calculation brought by the use of anchors makes detection and segmentation further towards real-time high precision.

Table 4 The evaluation index used in our experiment

Model	Evaluation index	LR	SR	HR
YOLOv4	Precision	58.5%	60.5%	65.5%
	Recall	65.0%	73.6%	79.5%
	mAP	60.7%	70.3%	76.4%
	Specificity	84.5%	89.5%	90.1%
CenterNet	Precision	51.6%	63.0%	68.4%
	Recall	52.9%	59.2%	62.5%
	mAP	58.1%	71.9%	76.3%
	Specificity	83.8%	82.6%	92.5%

As shown in Table 4, various indicators (precision, recall, and mAP) all indicate that although the super-resolution generated image has a certain distance from the original image, it is significantly better than the low-resolution image and achieves a relatively ideal effect. The accuracy improvement effect on CenterNet is better than YOLOv4, which also shows that the keypoint-based model is more dependent on the high resolution of the image than the anchor-based network.

The experiments also showed that the models cannot recognize certain lesion features or are prone to misjudgment due to unclear images, which may increase or decrease the Specificity score. Therefore, indicators such as Specificity cannot well represent the meaning of SR. However, the consistent high value of the Specificity indicates that the super-resolution model parameter adjustment is appropriate and effective.

C. MULTI-AI MODEL

Different from the general target detection models, we focus more on the model's reliability and helps to the doctor. Therefore, the multi-AI model will pay less attention on the computing speed and resources. In addition to custom RTP indicators, we also use FP (false positives) as evaluation indicators, which refers to the error that incorrectly indicates the presence of lesions. It should be noted that this is a classification task. We only need to analyze the rate of right classification on those labeled medical images as other images will be analyzed by the doctor. On this basis, we discarded some important indicators, such as sensitivity, recall, precision.

The confusion matrix is composed of TP, FP, TN, and FN. The result of a single classification model conforms to the following rules: the sum of TP and FN is 530, and the sum of FP and TN is 1300. However, the results of multi-AI model is uncertain:

$$\begin{cases} TP_{multi-AI} \leq TP_{yolov4} \cap TP_{centerNet} \\ TN_{multi-AI} \leq TN_{yolov4} \cap TN_{centerNet} \\ FP_{multi-AI} \leq FP_{yolov4} \cap FP_{centerNet} \\ FN_{multi-AI} \leq FN_{yolov4} \cap FN_{centerNet} \end{cases} \quad (6)$$

It can be seen from Eqn. (6) that the judgment of the multi-AI model is the part of the union of the sub-model results. The two thresholds set by Eqn. (2) make the judgment more demanding. Our experiments use the original image of the ultrasound data set as the input for this experiment, and the result of the confusion matrix is as follows:

Table 5 The confusion matrix of the models (modify the target detection model for classification)

Label Prediction \	Positive	Negative
Positive	306	129
Negative	224	1171

A) YOLOv4

Label Prediction \	Positive	Negative
Positive	332	97
Negative	198	1203

B) CenterNet

Label Prediction \	Positive	Negative
Positive	305	43
Negative	13	1038

C) YOLOv4+CenterNet

The images with benign and malignant tumors were treated as negative samples and those without lesions as positive samples. As shown in the two-class confusion matrix in Table 5, the performance is fair when using the feature map of the backbone of a single target detection model for classification. Single target classification model is prone to the missed detection, which makes the FN value too large. After combining YOLOv4 and CenterNet, the FN and FP values dropped significantly to the desired effect. Although the TP value also dropped, it is acceptable.

In the experiment, adjusting the threshold can control the multi-AI model's performance. Specifically, the stricter the threshold score was controlled, the less evaluation the multi-AI model can make; then the error rate is lower (FN and FP decrease), and vice versa. In actual situations, the FN is much more important than the TP. People who are misjudged as having the disease will receive doctors' second examination, while those who are misjudged will delay their treatment. Therefore, in the multi-AI model experiment, the FN score was controlled within a reasonable range.

In order to make the experimental results clearer, we define the sensitivity and specificity as shown in Eqn. (7):

$$\begin{cases} Sensitivity_{multi-AI} = \frac{TP_{multi-AI}}{TP_{multi-AI} + FP_{multi-AI}} \\ Specificity_{multi-AI} = \frac{TN_{multi-AI}}{TN_{multi-AI} + FP_{multi-AI}} \end{cases} \quad (7)$$

And the results were presented as follows:

Table 6 The metrics used in the experiment

Model	Sensitivity	Specificity	RTP
YOLOv4	57.73%	90.08%	100%
CenterNet	62.64%	92.54%	100%
YOLOv4+CenterNet	95.91%	96.02%	76.45%

From Table 5 and Table 6, we can see that the model is more conservative in the positive judgment of the disease, which makes sensitivity low and specificity high. This will reduce the correct positive diagnosis; yet it will also reduce the misdiagnosis rate, making the entire model more reliable.

As showed in the experimental results of a single target detection model, applying them to medical image detection requires constant modification and adjustment of parameters and even modification of the framework. The idea of the joint model allows them to play an effect far exceeding that of a single model, which validates a new idea for medical image detection.

All in all, the good performance of related indicators show that the multi-AI model is very reliable compared to the single target detection model, which exactly helps the doctors.

V. Conclusions and future work

The super-resolution experiments performed well in imaging quality and detection effects. Yet, the low-resolution images were manually generated rather than collected from the ultrasound equipment, leading the model generalization slightly insufficient. The super-resolution model also employed the VGG network, therefore, this part can also complete classification tasks or participate in evaluation as a subsystem.

Although the multi-AI model can reduce the doctors' workloads as showed in the experiments, the workload would still be very heavy when the input data size is large. In this case, the score of the indicator RPT will drop. It was assumed that the more "members" in the combination model, the more difficult it is to reach a consistent opinion; thus, we only included two "members". We may make the final decision through a voting system or by multiple members according to their weight. From this perspective, the multi-AI model provides a feasible solution and verifies the feasibility.

Finally, how the neural network model serves medical images is based on the purpose. Here we use the detection model for classification, which is actually a very practical tip. Although many model improvements are based on the combination of channels or feature maps, apart from the percentage increase or decrease in the evaluation score, they have not brought much substantial help to doctors. Unless a single model can approach 100% accuracy, it is difficult to bring AI models into practice in the field of medical imaging.

ACKNOWLEDGMENT

The authors thank the Peking University Shenzhen Hospital for providing the breast cancer image data and support of image analysis. The authors thank the Shenzhen Science and Technology Project (NO.JSGG20191129103020960) for supporting this research.

REFERENCES

1. Ferlay J, Soerjomataram I, Dikshit R, et al. Cancer incidence and mortality worldwide: Sources, methods and major patterns in GLOBOCAN 2012. *International Journal of Cancer* 2015;136: E359–E386.
2. Estimating the global cancer incidence and mortality in 2018: GLOBOCAN sources and methods - Ferlay - 2019 - International Journal of Cancer - Wiley Online Library, <https://onlinelibrary.wiley.com/doi/full/10.1002/ijc.31937> (accessed 19 December 2020).

3. Marmot MG, Altman DG, Cameron DA, et al. The benefits and harms of breast cancer screening: an independent review. *British Journal of Cancer* 2013; 108: 2205–2240.
4. Shin HJ, Kim HH, Cha JH. Current status of automated breast ultrasonography. *Ultrasonography* 2015; 34: 165–172.
5. Calas MJG, Almeida RMVR, Gutfilen B, et al. Intraobserver interpretation of breast ultrasonography following the BI-RADS classification. *European Journal of Radiology* 2010; 74: 525–528.
6. Jarosik P, Lewandowski M. The feasibility of deep learning algorithms integration on a GPU-based ultrasound research scanner. In: *2017 IEEE International Ultrasonics Symposium (IUS)*. 2017, pp. 1–4.
7. Chakraborty M. *Fog Computing Vs. Cloud Computing*. SSRN Scholarly Paper ID 3414500, Rochester, NY: Social Science Research Network. Epub ahead of print 3 May 2019. DOI: 10.2139/ssrn.3414500.
8. Mahmoudzadeh A, Kashou N. Interpolation-based super-resolution reconstruction: effects of slice thickness. *Journal of medical imaging*. Epub ahead of print 2014. DOI: 10.1117/1.JMI.1.3.034007.
9. Park JH, Choi W, Yoon GY, et al. Deep Learning-Based Super-resolution Ultrasound Speckle Tracking Velocimetry. *Ultrasound in Medicine & Biology* 2020; 46: 598–609.
10. Dong C, Loy CC, He K, et al. Learning a Deep Convolutional Network for Image Super-Resolution. In: Fleet D, Pajdla T, Schiele B, et al. (eds) *Computer Vision – ECCV 2014*. Cham: Springer International Publishing, 2014, pp. 184–199.
11. Redmon J, Divvala S, Girshick R, et al. You Only Look Once: Unified, Real-Time Object Detection. pp. 779–788.
12. Bochkovskiy A, Wang C-Y, Liao H-YM. YOLOv4: Optimal Speed and Accuracy of Object Detection. *arXiv:200410934 [cs, eess]*, <http://arxiv.org/abs/2004.10934> (2020, accessed 22 December 2020).
13. Liu S, Huang D, Wang andYunhong. Receptive Field Block Net for Accurate and Fast Object Detection. pp. 385–400.
14. Girshick R, Donahue J, Darrell T, et al. Rich Feature Hierarchies for Accurate Object Detection and Semantic Segmentation. pp. 580–587.
15. Ren S, He K, Girshick R, et al. Faster R-CNN: Towards Real-Time Object Detection with Region Proposal Networks. *IEEE Transactions on Pattern Analysis and Machine Intelligence* 2017; 39: 1137–1149.
16. Redmon J, Farhadi A. YOLO9000: Better, Faster, Stronger. pp. 7263–7271.
17. Redmon J, Farhadi A. YOLOv3: An Incremental Improvement. 5.
18. Liu W, Anguelov D, Erhan D, et al. *SSD: Single Shot MultiBox Detector*.
19. Lin T-Y, Goyal P, Girshick R, et al. Focal Loss for Dense Object Detection. pp. 2980–2988.

20. Zhang X, Lin X, Zhang Z, et al. Artificial Intelligence Medical Ultrasound Equipment: Application of Breast Lesions Detection. *Ultrason Imaging* 2020; 42: 191–202.
21. Duan K, Bai S, Xie L, et al. CenterNet: Keypoint Triplets for Object Detection. pp. 6569–6578.
22. Law H, Deng J. CornerNet: Detecting Objects as Paired Keypoints. pp. 734–750.
23. Ha I, Kim H, Park S, et al. Image retrieval using BIM and features from pretrained VGG network for indoor localization. *Building and Environment* 2018; 140: 23–31.
24. Zhang Z, Zhang X, Lin X, et al. Ultrasonic Diagnosis of Breast Nodules Using Modified Faster R-CNN. *Ultrason Imaging* 2019; 41: 353–367.